Results of Some Recent Hydrofoil Work

ALAN C. CONOLLY*
General Dynamics/Convair, San Diego, Calif.

Subcavitating and supercavitating hydrofoils were tested in the high-speed towing basin in a long-term research effort. In the subcavitating program, a zero dihedral hydrofoil model fitted with various sizes of hinged flaps was tested in smooth water, then with flaps cycling in smooth water, fixed in waves, and finally cycling in waves. For the first part of the supercavitating investigation, the performance of two hydrofoil sections without flaps was compared in smooth water, and, for the second part, two sections were tested with various sizes of split flaps in smooth water. For the subcavitating tests in smooth water, reasonable agreement is shown between the measured flap data and aerodynamic theory. It is shown that the vectorial addition of the separate effects of fixed flaps in waves and driven flaps in smooth water is in close correlation with results for cycling flaps in waves. It is substantiated for supercavitating design that the Tulin two-term section has a greater lift-to-drag ratio than a flat wedge section at a given lift coefficient, and good flap effectiveness is obtained on supercavitating foils. Data at cavitation number zero agree with accepted theory.

Nomenclature

h = depth of foil below free surface
c = chord of hydrofoil
b = span of hydrofoil
V, U_∞ = model velocity
V_c = critical cavitation speed
C_L = hydrofoil lift coefficient
L = hydrofoil lift in pounds
C_D = hydrofoil drag coefficient
D = hydrofoil drag in pounds
C_f = frictional drag coefficient of hydrofoil
c_f = chord of flaps
b_f = span of flaps
α = angle of attack of foil
δ_f = angular deflection of flap
ΔC_L = incremental lift coefficient
ΔC_{L_1} = one-half amplitude of C_L fluctuation, flaps fixed in waves
ΔC_{L_2} = one-half amplitude of C_L fluctuation, flaps cycling in smooth water
ϕ_{L_1} = phase lag or lead angle of max C_L to wave peak
ϕ_{L_2} = phase lag or lead angle of max C_L to max flap-down position
ω_f = frequency of flap oscillation, rad/sec
A_K = wave one-half amplitude
$\Delta\delta_f$ = flap one-half amplitude of oscillation
ν = frequency of wave encounter, rad/sec
λ_K = wavelength
V_W = wave velocity
σ_v = cavitation number based on vapor pressure = $(p_0 - p_v)/\frac{1}{2}\rho V^2$
σ_c = cavitation number based on measured cavity pressure = $(p_0 - p_c)/\frac{1}{2}\rho V^2$
σ = theoretical cavitation number
ρ = density of water, slugs/ft^3
p_0 = freestream pressure (absolute)
p_c = cavity pressure (absolute)
p_v = vapor pressure of water
α_0 = angle of attack of hydrofoil for zero lift
$c_{L\alpha}$ = lift-curve slope at infinite submergence
$C_{l\alpha}$ = two-dimensional lift-curve slope
K_t = $(1 + \epsilon_1)/(1 + \epsilon_1^2)$ where $\epsilon_1 = 4/(3 \times 3^{1/2}) \times (t/c)$
E_c = Jones edge correction (wing semiperimeter/wing span)
τ = correction for nonelliptical planform
a, A = aspect ratio of hydrofoil
m = Green's solution for the lift-curve slope of a two-dimensional ventilated flat plate
α_c = angle of attack increase due to camber
α_i = induced angle of attack
α^1 = angle of attack measured from hydrofoil chord line (equals α for a flat plate)
ϵ = deviation of force vector from the normal (equals zero for a flat plate)
δ = foil angle of incidence in Lin's† theory
ϵ = flap angle in Lin's theory

Introduction

THE three basic types of hydrofoil sections are the subcavitating, the base-ventilating, and the supercavitating, each having its own special characteristics. However it is possible to construct a hydrofoil that combines some characteristics of the various types, and a hydrofoil such as this will have a greater operating speed range, although there may have to be some compromises (on lift over drag ratio, for example).

The subcavitating hydrofoil usually has the section of a high subsonic airfoil, and because of the analogy between Mach number and cavitation number, the characteristics that delay sonic effects also delay cavitation. The supercavitating hydrofoil has a wedge-shaped section with a sharp leading edge. It is designed so that a cavity emanates from the leading edge and completely envelopes the foil upper surface, extending several chords downstream. The lower surface does not cavitate because it is designed to operate at pressures greater than the ambient pressure. Such foils do not give such high lift over drag ratios as the subcavitating types but can operate up to extremely high speeds and are very stable at all of the speeds in the supercavitating regime. The base-vented hydrofoil has characteristics midway between the fully wetted and the supercavitating types. It is still susceptible to cavitation, but the critical speed at which cavitation begins can be delayed appreciably.

The three basic types of hydrofoils are illustrated in Fig. 1, together with their approximate speed regimes. The General Dynamics/Convair work described in this paper has been in the field of subcavitating and supercavitating hydrofoils.

The subcavitating hydrofoil tests were performed for the Office of Naval Research. The section chosen was the

Presented as Preprint 64-309 at the 1st AIAA Annual Meeting, Washington, D. C., June 29–July 2, 1964; revision received February 23, 1965. The test programs were sponsored by the Navy Bureau of Ships and the Office of Naval Research, under Contract Nos. NObs-84615 and NOnr-3180(00). The author wishes to acknowledge the work of all members of the Towing Basin Staff connected with the hydrofoil program and in particular the help given by R. H. Oversmith, Chief of Marine Sciences at General Dynamics/Convair.

* Senior Hydrodynamics Engineer, Marine Sciences Department.

† For other symbols in Lin's equations, refer to Ref. 11.

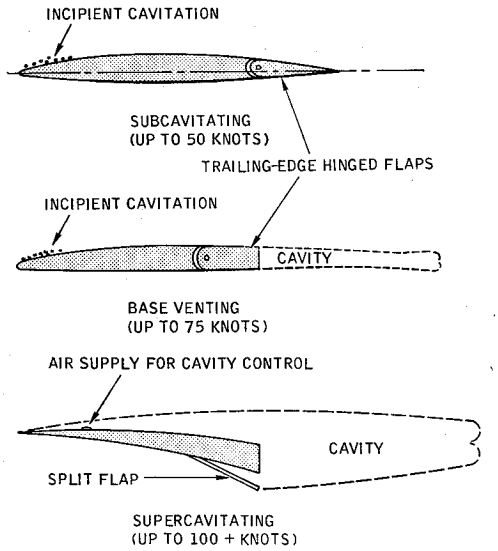

Fig. 1 Types of hydrofoils (diagrammatic).

NACA-16-309,[1] which was considered to be representative of sections suitable for a modern craft with fully submerged foils. (This actually is the foil section of the Navy's PC(H) "High Point.") The NACA 16-series sections[6,7] were designed to have a uniform chordwise pressure distribution at the design C_L with no violent suction peaks near the leading edge which would lead to early cavitation. The supercavitating hydrofoil tests were carried out for the Navy Bureau of Ships. Three sections were used, the first a flat wedge, the second a Tulin two-term section developed at Hydronautics Inc., and the third a modified version of the Tulin two-term section known as the BuShips supercavitating parent foil.

To find the effectiveness of flaps on hydrofoils, the subcavitating section was tested with various sizes of plain hinged flaps, and the supercavitating sections were tested with a range of trailing-edge, lower-surface split flaps. The test program was conducted at the Convair Hydrodynamic towing basin, which is 300 ft long, 12 ft wide, and 6 ft deep.

Flapped Hydrofoils in Smooth Water: Subcavitating Flow[2]

The first experimental work was the testing in smooth water of a subcavitating hydrofoil of 24-in. span and 4-in. chord with an aspect ratio of 6 and an NACA 16-309 section. It was mounted to the traveling carriage by a single strut. It was designed to be fitted with various sizes of simple hinged trailing-edge flaps and was instrumented to measure hydrofoil lift, drag and pitching-moment coefficients, and also flap lift, drag, and hinge moments. The model was constructed to allow the testing of four flap sizes, described in Table 1. Steel inserts were fastened to the model wing for configurations other than $c_f/c = 0.3$ and $b_f/b = 0.8$. Figure 2 is a photograph of the model with flap configuration 3.

The operating procedure consisted of testing the model over a range of velocities at a fixed depth of submergence of 4 in. (1 chord) measured from the wing quarter-chord. Wing

Table 1 Description of flap sizes for subcavitating foils

Model flap configuration	c_f/c	b_f/b
1	0.3	0.6
2	0.3	0.8
3	0.2	0.6
4	0.2	0.8

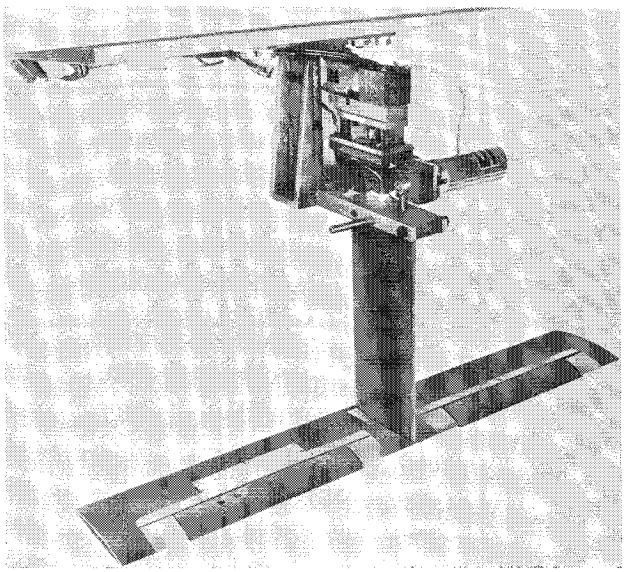

Fig. 2 Flapped subcavitating hydrofoil model with smallest flaps installed.

angles of attack were −5°, 0, 2°, 5°, and 10°. Flap deflection angles were −5°, 0, 2°, 5°, 10°, and 20°. Figure 3 shows typical C_L vs α curves for the model with flap configuration $c_f/c = 0.3$ and $b_f/b = 0.8$ at a depth of 1 chord. Flap lift increments were a little lower than predicted by theory (Fig. 4), and lift-curve slope was also slightly lower.

Flapped Hydrofoils in Waves: Subcavitating Flow[3]

The same subcavitating model was then tested in unsteady conditions. Tests were carried out separately with flaps oscillating in smooth water, flaps fixed in waves, and then various combinations of conditions with flaps oscillating in regular waves. The separate effects of flap and wave on the

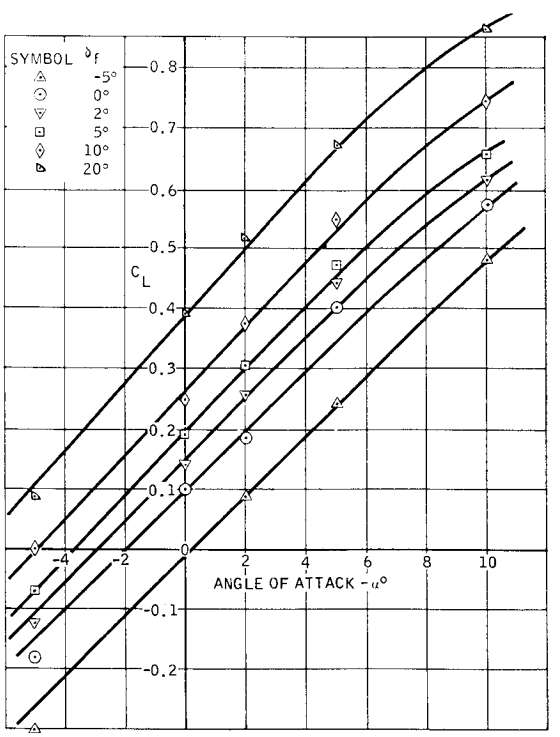

Fig. 3 Lift coefficient: model configuration 2, $c_f/c = 0.3$, $b_f/b = 0.8$, and $h/c = 1$.

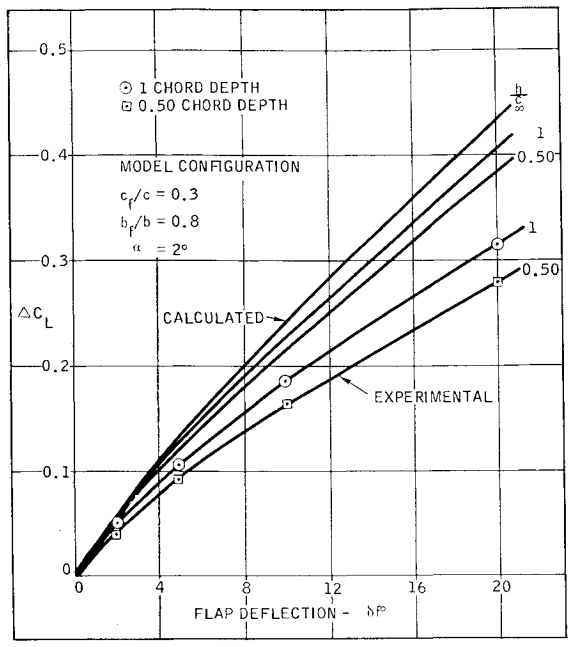

Fig. 4 Flap effectiveness at various depths: comparison of theory with experiment (model configuration 2).

force and moment coefficients for the hydrofoil were obtained and compared with the results when both flap and wave were cycled together.

Flap oscillation frequencies, which were constant for any given run, varied between 0.5 and 7.0 cps. Regular waves from the paddle-type wave maker, again constant for any run, were varied between 2 and 4 in. in height and between 3.5 and 8.25 ft in length (i.e., 20:1 to 24:1 approximately). Flap angles were varied through the range of $-8°$ to $+8°$ during cycling tests and between $-5°$ and $+10°$ for flaps fixed in wave tests. Positive values denote flaps deflected downward.

The procedure when testing with flaps cycling in waves was to choose a flap frequency, wave size, and model velocity such that the frequency of encounter with a wave was almost the same as the frequency of oscillation of the flap. Usually, two runs were carried out under identical conditions in order to get instantaneous phase relationships between flap-down and wave peak between π rad lag, progressing through the "in-phase" condition to π rad lead.

Figure 5 presents a typical plot of $\Delta C_{L_2}/\Delta\delta_f$ and ϕ_{L_2} (the phase of maximum C_L to the flap-down position) against a base of flap cycling frequency in radians per second for the model with flap configuration $c_f/c = 0.3$, $b_f/b = 0.8$ tested in smooth water. It will be noted that $\Delta C_{L_2}/\Delta\delta_f$ tends to increase with increase of flap cycling frequency, and this may mean that there is no flow separation at the higher frequencies.

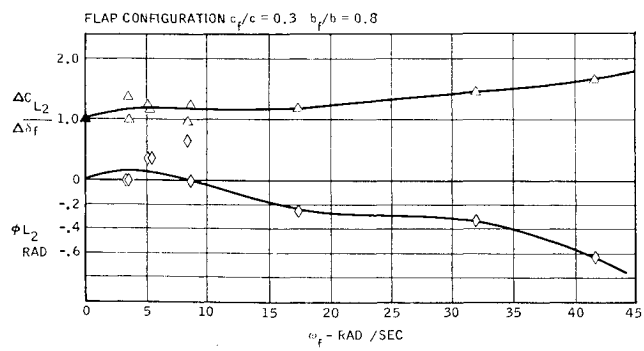

Fig. 5 Lift frequency response, flaps oscillating, smooth water.

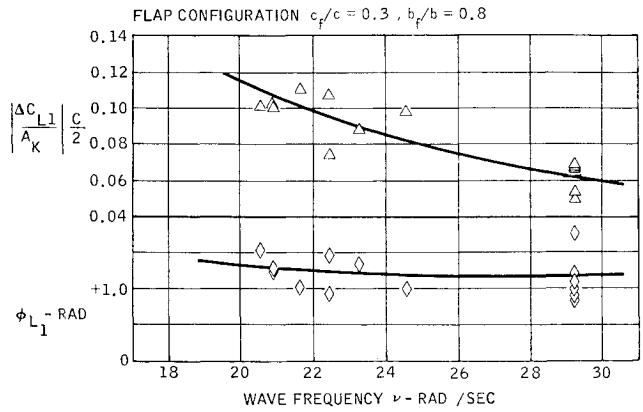

Fig. 6 Lift frequency response, head seas, flaps fixed.

Figure 6 presents a typical plot of the nondimensional coefficient $(\Delta C_{L1}/A_K)(c/2)$ and the phase of maximum C_L to the wave peak against a base of frequency of wave encounter in radians per second for the model with flap configuration $c_f/c = 0.3$, $b_f/b = 0.8$ in a head sea-condition.

It was observed that there was a pronounced difference in the phase relationships between head and following seas. Because of the orbital velocity of the wave, the maximum lift occurs approximately $\pi/2$ rad ahead of the wave peak in a head sea and approximately $\pi/2$ rad after the wave peak in a following sea. This is because of the change of effective angle of attack on the foil as it passes through the waves.

The frequency of wave encounter was defined as $\nu = (2\pi/\lambda_k)(U_\infty \pm V_W)$ rad/sec. The positive sign is taken with head seas and the negative sign with following seas.

The oscillatory lift parameter decreases slowly with increase of ν for all of the four flap configurations in a head sea and increases slowly for all of the configurations in a following sea. The plotting of data for flaps cycling in regular waves is complicated because there are two forcing functions (flap and wave) of different frequencies. The forces and moments not

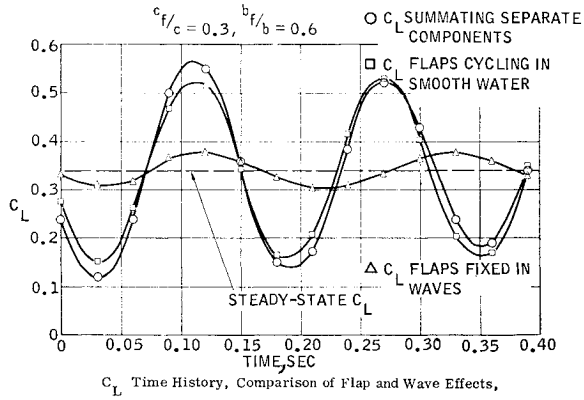

C_L Time History, Comparison of Flap and Wave Effects, Following Sea

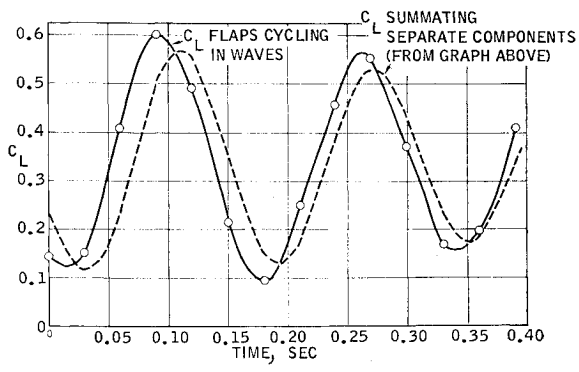

Fig. 7 C_L time history, following sea.

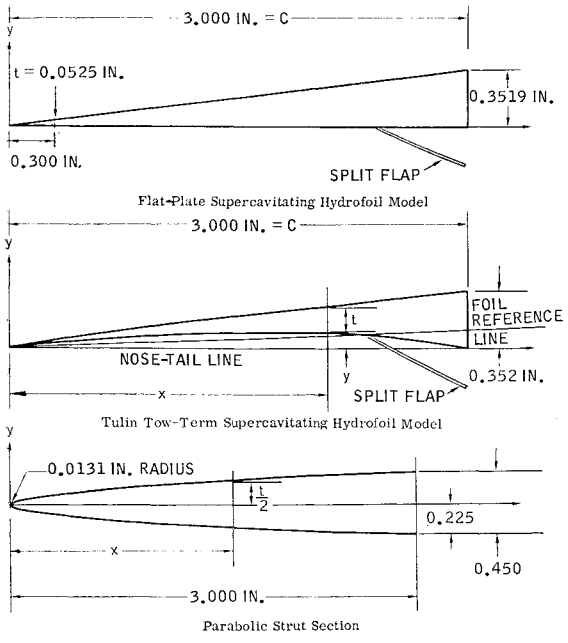

Fig. 8 Supercavitating sections (diagrammatic).

only have phase relationships with the wave, but different phase relationships with the flap. The oscillatory force and moment coefficients would vary with both frequency of wave encounter and frequency of flap oscillation, as well as with the phase relationship of the flap to the wave. Consequently, the best way to analyze these data is in terms of continuous time histories. Figure 7 shows the separate components of ΔC_L resulting from flap and ΔC_L caused by the wave for a following sea case for the foil with flap configuration c_f/c = 0.3, b_f/b = 0.6. The two effects are shown added together and compared with the same conditions where both flap and wave were cycled together. The wave frequency of encounter was 4.72 cps. The wave height (trough to crest) was 1.73 in. and its length 3.66 ft. The flap frequency was 6.30 cps.

C_L variation with flaps cycling in waves agrees very closely with C_L obtained by adding instantaneous components as follows: 1) component caused by flaps fixed in calm water, 2) component caused by flaps cycling in smooth water, and 3) component caused by flaps fixed in waves. Agreement is found in amplitude of oscillation, period, and reduction in amplitude (i.e., beating) on going from flap "lag" to "in-phase" conditions.

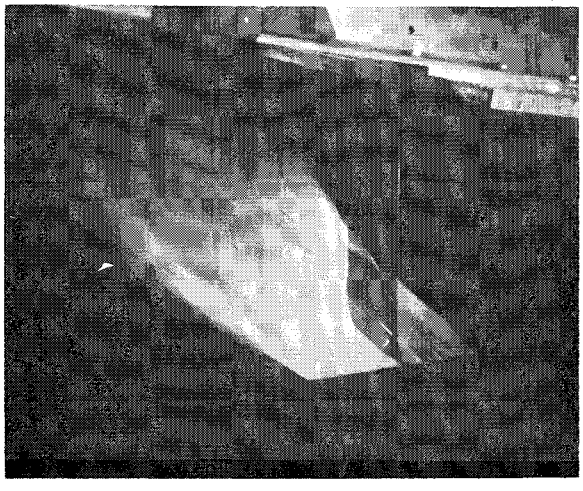

Fig. 9 Tulin two-term model in supercavitated flow.

Supercavitating Hydrofoil Studies[4]

The next phase of the experimental hydrofoil work was performed for the U. S. Navy Bureau of Ships and consisted of investigating two types of supercavitating hydrofoil sections. One was a $6\frac{1}{2}°$ flat wedge, and the other was a Tulin two-term section (Table 2). The foils were of rectangular planform with 9-in. span and 3-in. chord. Both were attached to a single supporting strut, which was parabolic in cross section, terminating in a blunt trailing edge. This provided an air entrainment path from the atmosphere to the upper surface of the hydrofoil. The two foil sections and the strut section are illustrated in Fig. 8. The section offsets were specified by BuShips. The two-term foil was designed (on the basis of two-dimensional flow at zero cavitation number) to operate at an angle of attack of 3.695° measured from the nose-tail line. At that design angle, it was predicted to develop a design lift coefficient of 0.275. However it was found to be not possible to operate this section supercavitated at an angle of attack below about $9\frac{1}{2}°$, because the flow would not separate cleanly from the foil upper surface. These high angles of attack caused low lift over drag ratios for the hydrofoil model.

In these present tests, the hydrofoil was instrumented to measure total lift, drag, and pitching moments. Hydrofoil twist and spanwise bending were also measured. Force and moment measurements were made for a range of angles of attack from 7.8° to 15.5° and for depths of submersion of 0.33, 0.67, and 1.00 times foil chord. Speed varied from 18 to 89 fps. At the lower speeds and angles of attack, the hydrofoil sections were operating base-vented.

Figure 9 shows a photograph of the two-term model in supercavitated flow at high speed. Figure 10 presents typical curves of C_L vs σ_v at angles of attack from 7.8° to 15.5° for the flat-plate foil at h/c = 1.00. Note that $\sigma_v = 2160/V^2$ approximately, and so high values of σ_v represent low values of speed. It can be seen that, for any given angle of attack, C_L in the base-vented condition is about double the C_L in the supercavitated condition, and also C_L varies with speed for supercavitated flow. At α = 7.8°, it was not possible to obtain supercavitated flow even at the highest speeds.

Figure 11 presents plots of L/D versus C_L for the supercavitating foils at σ_v = 0.3 and h/c = 0.33. The lower, shorter, curves are for fully ventilated conditions, i.e., where the cavity has broken open to the atmosphere. Under these conditions the cavity pressure approximates to atmospheric pressure, and the true cavitation number σ_c approaches zero. The experimental measurements showed that, at a vapor cavitation number of 0.3 and a depth/chord ratio of 0.33, the two-term foil has a lift-to-drag ratio of 5.9 at the design C_L of 0.275. For the same conditions, the flat-plate foil has a lift-to-drag ratio of 4.0.

Experimental Investigations of Supercavitating Hydrofoils with Flaps[5]

This phase was also sponsored by the U. S. Navy Bureau of Ships and consisted of investigating two types of supercavitating hydrofoil sections fitted with various sizes of split

Table 2 Ordinates for Tulin two-term section

x/c	x in.	y in.	t in.
0.050	0.150	0.013	0.016
0.100	0.300	0.027	0.024
0.200	0.600	0.053	0.038
0.300	0.900	0.073	0.054
0.500	1.500	0.093	0.107
0.700	2.100	0.082	0.178
0.900	2.700	0.036	0.286
1.000	3.000	0	0.352

trailing-edge flaps. The same models were used as in the previous tests, except that the two-term section was modified slightly to give it less camber and greater thickness toward the trailing edge to accommodate flaps and balances. Measurements were made of hydrofoil lift, drag, and pitching moments, as well as flap lift, drag, and hinge moments. Measurements were also made of flap deflection caused by the load on the flap and hydrofoil spanwise twisting. Five sizes of flaps on the two-term section enabled the separate effects of flap chord and span variation to be obtained. Table 3 shows the flap configurations that were tested. Flaps were split into two on both sides of the foil, making four flaps in all, except for the configurations $b_f/b = 0.7$ and $b_f/b = 0.45$ where only two flaps were used. Both starboard flaps were strain-gaged. Cavity pressure was measured for all of the models, and all of the cavities were obtained by high carriage speed and ventilation, which occurred down the back of the strut. Testing was done in smooth water. Data extrapolated to a cavitation number of zero were compared with the theory of Lin.[11] The experimental data agree quite well with previous work and, under fully ventilated conditions, with theoretical calculations.

The tests had to be carried out at very high angles of attack in order to obtain upper surface cavities, and these very high angles were associated with low lift-to-drag ratios in the order of 4.0.

Figure 12 shows typical data collected for the modified Tulin two-term foil with flap configuration $c_f/c = 0.4$, $b_f/b = 0.9$ at an angle of attack $\alpha = 11.7°$ and a depth/chord ratio $h/c = 1.00$. Curves of C_L and C_D are presented, plotted against σ_v, for constant flap deflections of 0, 5°, and 10°. It can be seen that C_L and C_D vary with speed in the supercavitating regime.

The split flap was found to be an effective way of increasing foil lift at a given angle of attack. Crossplots of the effects on hydrofoil force coefficients caused by changing flap size give a good indication of the optimum flap span and chord on the hydrofoil configuration tested. These values were flap chord/foil chord = 0.3, and flap span/foil span = 0.9. Figure 13 presents graphs showing the effect of flap geometry on C_L for an angle of attack of 11.7°, a depth/chord ratio of 0.67, and a cavitation number $\sigma_v = 0.4$.

Comparison of Subcavitating Hydrofoil Data with Aerodynamic Theory

The flap-neutral lift curve was calculated from $C_L = (\alpha - \alpha_0)C_{L\alpha}$ where $(\alpha - \alpha_0)$ is the wing angle of attack measured from zero lift, and

$$C_{L\alpha} = c_{l\alpha}\{K_t a/[E_c a + 2K_t(\tau + 1)]\}$$

The depth correction was from an empirical approximation by Tinney,[8] i.e.,

$$C_L/C_{L\infty} = 1 - 0.422\exp(-1.454\, h/c)$$

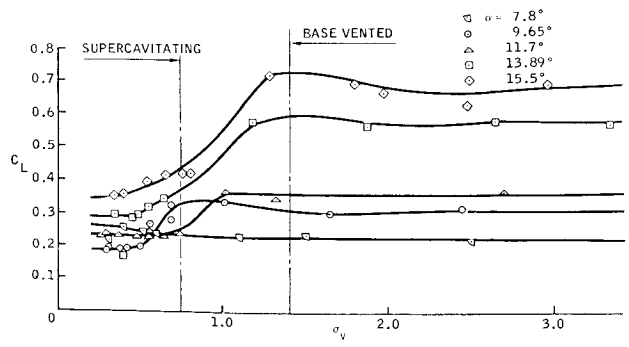

Fig. 10 Lift coefficient, $h/c = 1.00$ (flat-plate foil).

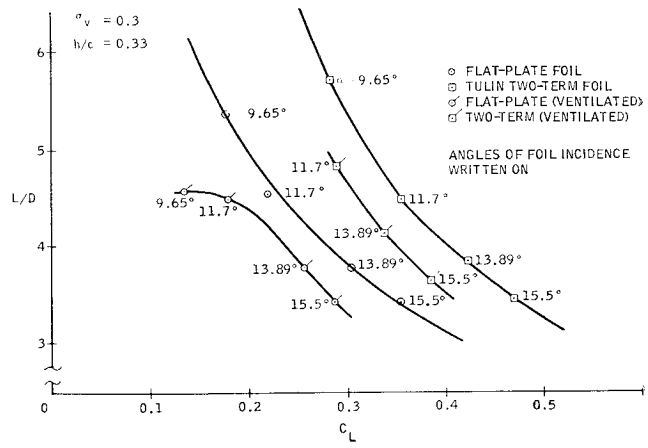

Fig. 11 Variation of lift-to-drag ratio with lift coefficient at $\sigma_v = 0.3$ and $h/c = 0.33$.

The hydrodynamic lift curves have slightly lower slopes than the corrected aerodynamic curves.

Flap Effectiveness

The lift coefficient of a flapped wing can be written as

$$C_L = C_{L\alpha}(\alpha - \alpha_0) + C_{L\delta_f}\delta_f$$

where $C_{L\delta_f}$ is the flap effectiveness. Thus

$$C_{L\delta_f} = f(c_f/c)f(\delta_f)f(b_f/b)f(\bar{h})$$

where the functions $f(c_f/c)$, $f(\delta_f)$, and $f(b_f/b)$ are corrections for flap geometry from Young.[9] The function $f(\bar{h})$ is a depth correction for a hydrofoil, and it is computed by a modification of Prandtl's lifting line theory as applied to the biplane. This pictures the hydrofoil and its image an equal distance above the water, i.e., a biplane with a gap distance of $2h$ and no wing stagger. The assumption is made that there is constant spanwise vorticity. For details of this derivation, see Jones.[2]

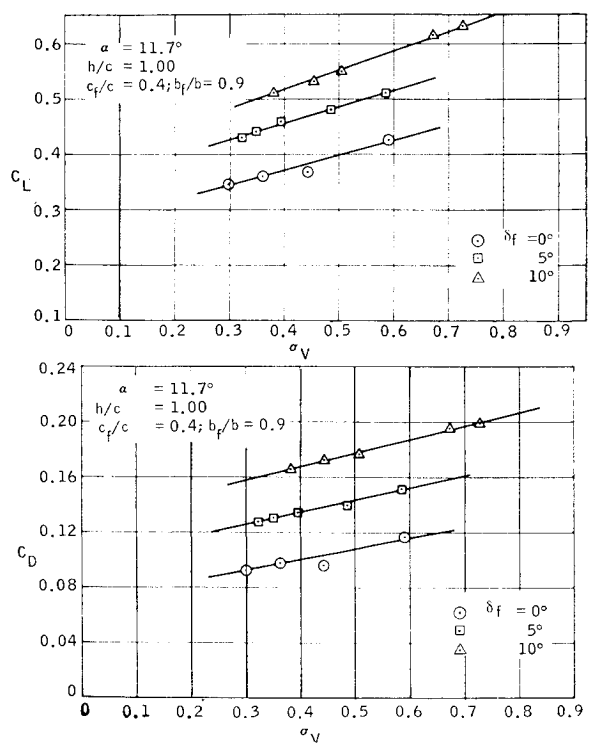

Fig. 12 Typical results for modified Tulin two-term foil with flaps (supercavitating parent foil).

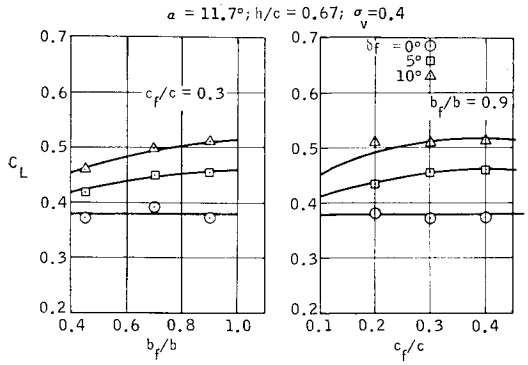

Fig. 13 Effect of flap geometry on C_L (supercavitating parent foil).

Figure 4 gives comparisons between theory and experiment for the hydrodynamic model with a flap configuration $c_f/c = 0.3$, $b_f/b = 0.8$. It shows the flap effectiveness at various depths and indicates that aeronautical theory predicts rather higher values of lift coefficient for a given flap angle than were obtained in this study.

Comparison of Supercavitating Hydrofoil Data with Theory for Zero Cavitation Number

All of the theoretical calculations are for $\sigma = 0$, i.e., where the cavity pressure is atmospheric, and all of the lift is obtained from the foil lower surface. This corresponds to the shallow-depth case in these present tests, where the cavity was completely open to the atmosphere. Only the performance of the flat-wedge foil has been checked theoretically.

Comparison with Johnson's Theory

Johnson[10] developed theoretical expressions for lift and drag developed for the zero cavitation number case. He checked these theoretical expressions with tests at the Langley tank, obtaining zero cavitation number by operating the foils near the water surface so that their upper surfaces were completely ventilated. His conclusions were firstly, that the theoretical force coefficients agreed with the data obtained in the tests

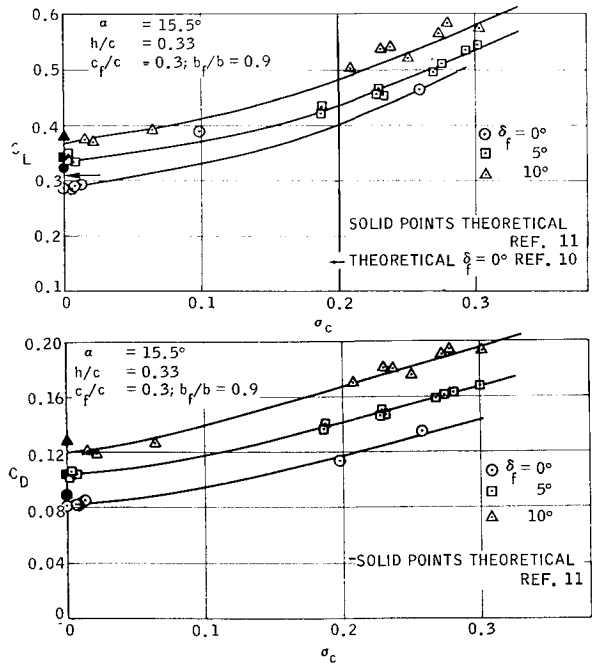

Fig. 14 Force coefficients with cavitation number based on measured cavity pressure (flat foil).

Table 3 Description of flap sizes for supercavitating foils

Model No. →	1	2	3	4	5	6
Foil section	Curved	Curved	Curved	Curved	Curved	Flat
c_f/c	0.2	0.3	0.3	0.3	0.4	0.3
b_f/b	0.9	0.7	0.45	0.9	0.9	0.9

within an accuracy of about 3%, and secondly, that the ventilated force coefficients were independent of speed. Johnson started with the work by Kirchoff and Rayleigh which provided formulas for the two-dimensional characteristics of an inclined flat plate in an infinite fluid at zero cavitation number. This work was modified by Green to include the effect of the free water surface, neglecting gravity. Johnson developed the following formula for the total lift on a finite aspect-ratio supercavitating hydrofoil operating near the free water surface:

$$C_L = \left[\frac{A}{A+1}\, m(\alpha + \alpha_c - \alpha_i)\, \frac{\cos\alpha}{\cos(\alpha - \alpha_c - \alpha_i)}\right] + \underbrace{\left[\frac{1}{A+1}\, 0.88\, \sin^2(\alpha^1 + \alpha_c)\cos\alpha^1\right]}_{\text{crossflow lift } C_{L,c}}$$

where $m = C_L/\alpha$ from Green's solution for the lift-curve slope for a two-dimensional ventilated flat plate. The drag coefficient

$$C_D = C_{L,\,1}\tan(\alpha + \epsilon) + C_{L,\,c}\tan\alpha^1 + C_f$$

where $C_{L,\,1}$ is the first term in the C_L equation.

Values of C_L, C_D, and L/D were calculated for the flat-plate hydrofoil at flap deflection zero, angles of attack of 4°, 11.7°, 13.8°, and 15.5°, and depth/chord ratios of 0.33, 0.67, 1.00, and 1.50. The values are shown to be in close agreement with the experimental results (Fig. 14).

Figure 15 is a theoretical curve of L/D vs C_L for $h/c = 0.33$ and $\sigma = 0$. The experimental points lie very close to the curve and show that theory predicts these very low lift-to-drag ratios of about 4.0 at the high angles of attack used in the tests.

Comparison with Lin's Theory

To cover the flap case, Lin[11] extended Johnson's approximate method for calculating nonlinear lift and drag coefficients for cambered hydrofoils. He found the result of Johnson's method to be in very close agreement with the exact solution for moderate angles of incidence and flap angles and stated that, in the absence of an exact analysis for the finite depth case, Johnson's method should give a useful and accurate prediction of the lift and drag coefficients.

Green's formula was modified for the flap problem as follows:

$$\begin{aligned} C_L(\delta, \epsilon) &= 2\{b - (b^2 - 1)^{1/2}\}\, \sin\alpha_e\, (\cos\alpha/D) \\ &= m_e\alpha_e(\cos\alpha/\cos\alpha_e) \\ C_D(\delta, \epsilon) &= 2\{b - (b^2 - 1)^{1/2}\}\, \sin\alpha_e\, (\sin\alpha/D) \\ &= C_L(\delta, \epsilon)\, \tan(\alpha + \beta) \end{aligned}$$

$$D = \{b - (b^2 - 1)^{1/2}\sin\alpha_e + \frac{1}{\pi}\Big[2\cos\alpha_e + (b\cos\alpha_e - 1)\log\frac{b-1}{b+1}\Big]$$

Lin[11] gives examples of the calculations required. Note that the calculations are for $\sigma = 0$, and the flaps are assumed to be full span. A significant part of the computation requires data given by Auslaender,[12] and many useful graphs are given in this report.

The theoretical points have been plotted on the graphs of C_L vs σ_c and C_D vs σ_c for the flat-wedge hydrofoil (Fig. 14)

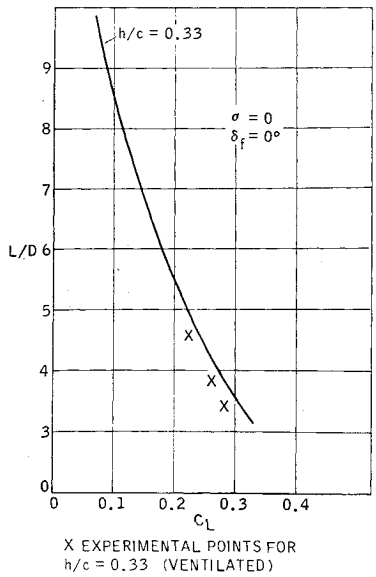

Fig. 15 Theoretical lift-to-drag ratio with C_L (flat foil).

and are seen to be in close agreement with the experimental results, both as regards to actual values of force coefficients and to incremental values caused by flap deflection.

Conclusions

For the subcavitating hydrofoil, the study demonstrated that flapped airfoil data may be used to predict the forces and moments on the submerged foil and flap if a depth correction is used.

The hydrofoil lift-curve slope is not affected by flap deflection and retains its linearity up to an angle of attack of nearly 10°, using the maximum sized flap of $c_f/c = 0.3$ and $b_f/b = 0.8$.

It was shown theoretically and experimentally that flap effectiveness decreases with decrease in depth of submergence. When the flap is cycling, the oscillatory lift coefficients and the oscillatory drag coefficients are not apparently affected by mean flap deflection or angle of attack within the range of $-5°$ to $+10°$

The average values of lift, drag- and pitching-moment coefficients in unsteady flow do not vary much from the equivalent steady-state conditions. It is possible to isolate and evaluate the separate effects of flap and wave motion and then add these vectorially to get the combined effects of flap and wave acting together.

The supercavitating test program showed the superiority of the two-term hydrofoil over the flat wedge. The two-term foil has a lift-to-drag ratio of 5.9 when operating at its design lift coefficient of 0.275 at $\sigma_v = 0.3$ and $h/c = 0.33$. At the same lift coefficient, the flat-plate foil has a lift-to-drag ratio of 4.0.

It was not possible to operate either foil at set angles of attack below $9\frac{1}{2}°$, measured to the nose-tail line of the foil lower surface, without wetting their upper surfaces. It appears that successful operation of supercavitating hydrofoils at low angles of attack will depend largely upon the design of the foil's upper surface. Flow separation must occur at the foil leading edge.

The split flap is an effective way of increasing foil lift at a given angle of attack. Deflecting the flap 10° produces more lift than increasing the angle of attack from 11.7° to 15.5°. The lift-curve slopes of the C_L vs α curves for the supercavitating foils are only about one half of those for efficient subcavitating foils. However, the foils can be operated at extremely high angles of attack without any apparent possibility of a stall.

It has been shown that the data agreed quite well with theoretical calculations for zero cavitation number under fully ventilated conditions, based on theory by Johnson[10] and Lin.[11]

Although subcavitating hydrofoils can now be designed with confidence, it is another story with supercavitating hydrofoils. Great strides have been made in acquiring experimental data and theoretical understanding of supercavitating hydrofoils, but many problems remain to be solved before they can become a practical reality for hydrofoil boats. For one thing, some means must be found to enable operation at low angle of attack and thus to obtain reasonably high lift-to-drag ratios. It has been demonstrated that even at high angles of attack supercavitating foils will not cavitate if the speed is too low. As the angle of attack goes down, the speed at which a cavity is formed rises; but there may be a limit to this. At sufficiently low angles of attack the upper surface of the foil will probably prevent the formation of a cavity at any speed. Added to this is a problem of hysteresis in cavity formation if speed is fluctuated near the critical speed. Another problem is that of scaling factors. Different conditions exist on the lower and upper surfaces of the foil. Cavity pressure is known to vary at different places within the cavity, and cavitation number based on some arbitrary pressure may not be meaningful for design purposes.

Split trailing-edge flaps are a useful way of increasing lift on the foil, but some means must be found for decreasing lift also. One way would be to vary upper surface cavity pressure by some means, but it has been demonstrated that the lift cavitation number curve slope is rather low, and this pressure might be tricky to control accurately.

Then there is the problem of operation in rough water with all of its attendant variations of conditions, and so it can be seen that the supercavitating hydrofoil will challenge the engineer and the mathematician for quite a while into the future.

References

[1] Jones, C. E., Jr., "Flapped hydrofoils in smooth water—subcavitating flow, Pt. 1 Hydrofoil selection," General Dynamics/Convair Rept. ZH-146 (July 1960).

[2] Jones, C. E., Jr., "Flapped hydrofoils in smooth water—subcavitating flow," General Dynamics/Convair Rept. ZH-153 (November 1961).

[3] Conolly, A. C., "Flapped hydrofoils in waves, subcavitating flow," General Dynamics/Convair Rept. GDC-63-032 (May 1963).

[4] Jones, C. E., Jr., "Supercavitating hydrofoil studies," General Dynamics/Convair Rept. GDC-63-021A (February 1963).

[5] Conolly, A. C., "Experimental investigations of supercavitating hydrofoils with flaps," General Dynamics/Convair Rept. GDC-63-210 (December 1963).

[6] Stack, J., "Tests of airfoils designed to delay the compressibility burble," NACA Rept. 763 (1943).

[7] Lindsey, W. F., Stevenson, D. B., and Daley, B. N., "Aerodynamic characteristics of 24 NACA 16-series airfoils at Mach numbers between 0.3 and 0.8," NACA TN 1546 (December 1947).

[8] Tinney, E. R., "Experimental and analytical studies of dihedral hydrofoils," St. Anthony Falls Hydraulic Lab., Univ. of Minnesota, Project Rept. 41 (1954).

[9] Young, A. D., "The aerodynamic characteristics of flaps," British Aeronautical Research Council, R&M 2622 (February 1947).

[10] Johnson, V. E., Jr., "Theoretical and experimental investigation of arbitrary aspect ratio, supercavitating hydrofoils operating near the free water surface," NACA RM L 57 I 16 (December 1957).

[11] Lin, J. D., "A free streamline theory of flows about a flat plate with a flap at zero cavitation number," Hydronautics, Inc. TR 119-3 (December 1961).

[12] Auslaender, J., "The behavior of supercavitating foils with flaps operating at high speed near a free surface," Hydronautics Inc. TR 001-2 (July 1960).